Available online at www.sciencedirect.com
SCIENCE DIRECT®
Physics and Chemistry of the Earth 29 (2004) 495–500
PHYSICS and CHEMISTRY of the EARTH
www.elsevier.com/locate/pce

Numerical analysis on the propagation of ULF/ELF signals in the lithosphere with highly conductive layers

Anton V. Kulchitsky [a], Yoshiaki Ando [b,*], Masashi Hayakawa [b]

[a] *Geophysical Institute, University of Alaska, Fairbanks, AL, USA*
[b] *The University of Electro-Communications, 1-5-1 Chofugaoka, Chofu, Tokyo 182-8585, Japan*

Received 10 July 2003; received in revised form 27 October 2003; accepted 30 October 2003
Available online 15 April 2004

Abstract

This paper deals with the numerical analyses on the effect of inhomogeneities (highly conductive layers) on the propagation of seismogenic electromagnetic signals in the ULF/ELF range. For simplicity of computations we assume that the geometrical configuration is uniform in one direction, which is possibly consistent with the actual situation. We adopt the frequency domain finite difference method in the computation, and calculate the electric field at points where the fields are measurable. Our numerical results show some significant findings: (1) it is necessary to consider the presence of air region in the lithospheric propagation, (2) there exist characteristic frequencies at which we have the effective response at a point due to the presence of the conductive layer, (3) a site closest to the source does not necessarily show the strongest response, depending on the configuration of the layers.

1. Introduction

There have been recently accumulated a lot of evidence on the presence of electromagnetic emissions in a wide frequency range from DC to VHF, associated with earthquakes (Hayakawa and Fujinawa, 1994; Hayakawa, 1999; Hayakawa and Molchanov, 2002), which would be of potential use for the short-term earthquake prediction. The long history of DC current measurement, so-called VAN method, has yielded interesting physical implications, and one typical example is the presence of selective site. This selectivity means that an observing station closest to the source cannot always detect the strongest signal, which suggests the presence of an inhomogeneity (fault) in the lithosphere and its effect on the propagation of DC seismogenic signals (Varotsos et al., 1998; Varotsos et al., 2000; Sarlis et al., 1999). These authors have also dealt with different orientations of the source, and it was shown that some interesting results can be obtained if the source is perpendicular to the conductive layer.

As compared with the DC study, the study of seismogenic ULF emissions has a short history since 1990, but there have been a few convincing reports on the presence of precursory ULF signatures for large earthquakes (Kopytenko et al., 1990; Fraser-Smith et al., 1990; Molchanov et al., 1992; Hayakawa et al., 1996; Hayakawa et al., 2000; Uyeda et al., 2002; Gotoh et al., 2002). A few generation mechanisms have been proposed for ULF seismogenic emissions, including the microfracturing mechanism (Molchanov and Hayakawa, 1995), but the propagation has not been extensively studied. Of course, there is a paper on the propagation of electromagnetic waves from the lithosphere to the atmosphere and ionosphere (Molchanov et al., 1995; Tian and Hata, 1996). The purpose of this paper is to investigate numerically the effect of any inhomogeneity in the lithosphere as suggested in the DC study on the propagation of ULF and ELF seismogenic emissions.

A few typical examples of the inhomogeneity in the lithosphere are treated in this paper; (1) a simple model of a fault with and without the presence of air region, (2) a generalized composite structure representing oceanic lithosphere colliding and subducting beneath the continental lithosphere. And we take a line current located inside or outside the inhomogeneities, because the seismogenic ULF source which is caused by microfractures, seems to be aligned along a strike. The problems are then reduced to two-dimensional cases from the

* Corresponding author. Tel.: +81-424-43-5160; fax: +81-424-43-5783.
E-mail address: ando@whistler.ee.uec.ac.jp (Y. Ando).

1474-7065/$ - see front matter © 2004 Elsevier Ltd. All rights reserved.
doi:10.1016/j.pce.2003.10.003

geometry mentioned above, and are formulated by the frequency domain finite difference (FDFD) method in complex field. The modeling and formulation will be given in Section 2, and we will make some case studies on seismogenic ULF fields on the ground surface in Section 3.

2. Mathematical simulation

2.1. Lithospheric modeling

There are two important points to model the Earth's crust for our analysis of the seismogenic ULF/ELF fields; the inhomogeneity of the crust as a propagation medium, and the spatial structure of the source.

The inhomogeneity of conductivity of the Earth's crust is quite complicated. But for the case of ULF/ELF fields which have an extremely long wavelength, we may ignore the effect of small inhomogeneities such as massive sulfide deposits, crustal fluid distribution, etc., so that we consider the net parameter of the medium. The significant inhomogeneity is a large-scale one near the seismogenic ULF/ELF emission source and the propagation paths to the ground surface. In this study our attention is paid to the presence of faults, subduction, and sea water, which are main inhomogeneities of our interest, because their location is very close to the source. It is known from the magnetotelluric sounding that there exist fault-zone conductors (FZCs) which are produced by crustal fluids. It was also reported that a relatively conductive zone was subducted beneath the lithosphere, and this seems to be sediment including sea water (Hermance, 1995).

As a source to generate seismogenic ULF/ELF fields, we consider a line current at the shallow depth of the Earth's crust, and let the line current run parallel to the strike. Though this source is introduced for the simplicity of calculation, it may sufficiently simulate the microfracturing to occur linearly because the stress to induce the microfracturing is planar or linear and is parallel to the inhomogeneity discussed above. There are a few other possible source mechanisms such as electrokinetic effect. However, we do not pay attention to the the source nature, but only to the propagation properties of the media.

In our analysis, the curvature of the Earth's surface is neglected and the flat ground is assumed because the phenomena under consideration is limited in the local region (<100 km). The system of the problem is reduced to two-dimensional one by assuming that this geometry continues infinitely along $\pm z$-direction and invoking that the line current is quasi-static.

Consequently, an example of the modeled configuration and the coordinates of the problem may be given as shown in Fig. 1. The origin of the coordinates is set at the position of a line source. The highly conductive layer is put vertically and extended infinitely. This example consists of three parts with different conductivity; the host region (σ_{H}), the layer (σ_{L}), and the air region ($\sigma = 0$).

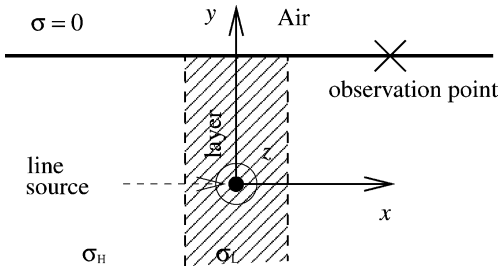

Fig. 1. Typical configuration for our analysis and the used coordinates system.

2.2. Mathematical formulation of our problem

The vector wave equation with respect to the electric field $\boldsymbol{E}(\boldsymbol{r})$, with the time factor $\mathrm{e}^{-\mathrm{i}\omega t}$ is given by

$$\nabla \times \nabla \times \boldsymbol{E}(\boldsymbol{r}) - \{\omega^2/c^2 + \mathrm{i}\omega\mu_0\sigma(\boldsymbol{r})\}\boldsymbol{E}(\boldsymbol{r}) = \mathrm{i}\omega\mu_0\boldsymbol{j}(\boldsymbol{r}), \tag{1}$$

where ω, c, μ_0, and $\sigma(\boldsymbol{r})$ are the angular frequency, the velocity of light, the permeability in vacuo and the conductivity, respectively. The current density $\boldsymbol{j}(\boldsymbol{r})$, can be expressed in terms of the Dirac's delta function:

$$\boldsymbol{j}(\boldsymbol{r}) = I\delta(x)\delta(y)\hat{\boldsymbol{z}}, \tag{2}$$

where I is the current intensity.

It is evident from the geometrical configuration that only the TE mode(E_z, B_x, B_y) is excited in the system. Letting $\boldsymbol{E}(\boldsymbol{r}) = E(\boldsymbol{r})\hat{\boldsymbol{z}}$, we obtain the reduced scalar wave equation:

$$\frac{1}{\mu_0}\left(\frac{\partial^2 E}{\partial x^2} + \frac{\partial^2 E}{\partial y^2}\right) + \omega^2\epsilon_0 E + \mathrm{i}\omega\sigma E = \mathrm{i}\omega I\delta(x)\delta(y). \tag{3}$$

The magnetic flux density $\boldsymbol{B}$, can be derived in terms of E as follows:

$$B_x = -\frac{\mathrm{i}}{\omega}\frac{\partial E}{\partial y}, \qquad B_y = \frac{\mathrm{i}}{\omega}\frac{\partial E}{\partial x}. \tag{4}$$

We introduce a new variable $\mathscr{E} = E/(\mathrm{i}\omega\mu_0)$ for the convenience of computation, so that the basic equation to be solved is rewritten as,

$$\frac{\partial^2 \mathscr{E}}{\partial x^2} + \frac{\partial^2 \mathscr{E}}{\partial y^2} + \left(\frac{\omega^2}{c^2} + \mathrm{i}\omega\sigma\mu_0\right)\mathscr{E} = I\delta(x)\delta(y). \tag{5}$$

There are two advantages to use the function $\mathscr{E}$; (1) the order of this function is nearly unity, and (2) this function changes slowly if we sweep frequencies of interest. The latter saves the computational time to solve the matrix generated by the FDFD by means of an iterative method when we calculate frequency charac-

teristics because we can utilize the result of the previous calculations as the initial values for the next step of iteration.

In the finite difference formulation, it is convenient from the geometry to adopt the rectangular mesh. The second order finite-difference numerical scheme can be derived readily as follows:

$$\frac{\Delta y}{\Delta x}(\mathscr{E}_{k+1,m} - 2\mathscr{E}_{k,m} + \mathscr{E}_{k-1,m}) + \frac{\Delta x}{\Delta y}(\mathscr{E}_{k,m+1} - 2\mathscr{E}_{k,m} + \mathscr{E}_{k,m-1}) + \Delta x \Delta y(\omega^2/c^2 + \mathrm{i}\omega\mu_0\sigma_{k,m})\mathscr{E}_{k,m} = I\delta_{k,m}, \quad (6)$$

where Δx and Δy are the size of each cell in x- and y-direction, respectively, and $\mathscr{E}_{k,m}$ indicates the function $\mathscr{E}(\boldsymbol{r})$ at the position $\boldsymbol{r} = (k\Delta x, m\Delta y)$ in the discretized nodes. $\delta_{k,m}$ is the Kronecker's delta. In order to truncate the mesh, the first order absorbing boundary condition is implemented at the analysis region boundaries (Jin, 1993). The successive over relaxation (SOR) method is effective to obtain iterative solutions of the huge matrix generated by the finite difference procedure in Eq. (6) (Press et al., 2002).

3. Numerical results and discussion

In this section we demonstrate some numerical results to study the general characteristics of the propagation of seismogenic ULF/ELF field. In Section 3.1 we verify the necessity to take into account the atmosphere, and in Section 3.2 and 3.3 we consider the influence of highly conductive layers on the ULF/ELF propagation.

3.1. Influence of the atmosphere

At first, we demonstrate the influence of the presence of atmospheric (air) region on the ULF/ELF propagation. Although they did not consider the presence of atmosphere in some previous investigations, and calculated the field in the full space with conductivity (we call it full-space model), the realistic model must consist of one half conductive region and another half, air region (semi-space model), and it is important in practice to consider the atmospheric influence because we can only measure the ULF/ELF fields at the boundary between the atmosphere and lithosphere. The size of conductive zones is not still well understood (see Hermance, 1995), but we consider a rather wide zone ranging from 1.5 to 4.5 km with comparably less conductivity to approximate this very inhomogeneous layers.

Fig. 2 shows the spatial profile of the ratio of the electric fields at the ground surface for the full-space model, E_{full}, to the semi-space model, E_{semi}. The conductivity of the host medium of both models is $\sigma_{\mathrm{H}} = 10^{-5}$ S/m, and the source is located at the depth of 15 km. The cell size is chosen as $\Delta x = \Delta y = 0.25$ km, and there are 1120×1120 cells in the analysis region

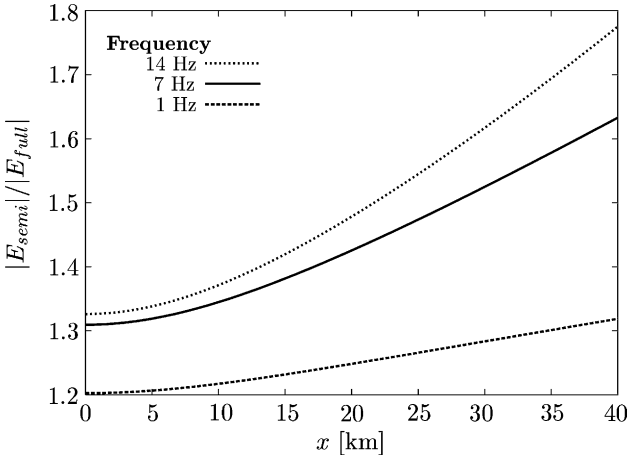

Fig. 2. Profile of the ratio $|E_{\mathrm{semi}}/E_{\mathrm{full}}|$ on the ground surface as a parameter of frequency.

($= 140$ km $\times 140$ km) including the absorbing boundary layers.

It is seen from Fig. 2 that the ratio is greater than unity over all ranges at all frequencies, and that it grows with the increase in frequency. This comparison shows the importance of considering the influence of the atmosphere on the observed ULF/ELF field, and we note that if the observation point is far from the epicenter, the discrepancy is found to be more enhanced.

3.2. Influence of a highly conductive layer on the frequency characteristics

In this section we show some numerical results in the presence of a highly conductive layer. The analysis model is same as Fig. 1, where a semi-infinite layer with $\sigma_{\mathrm{L}} = 10^{-3}$ S/m is inserted vertically into the host medium with $\sigma_{\mathrm{H}} = 10^{-5}$ S/m. The line source is embedded at the center of the layer and at the depth of 15 km. The cell size is given by $\Delta x = \Delta y = 0.25$ km, and the analysis region covers 140 km $\times$ 140 km ($= 1120 \times 1120$ cells) along x- and y-direction, respectively.

Fig. 3 illustrates the frequency characteristics of the absolute value of the electric field $|E|$ at the ground surface as a parameter of the layer width for $I = 1$A. The observation point is at the center of the top of the vertical layer. We truncate two curves at the middle of the range because it costs computational time and the tendency is the same as the line of 1.5 km width (solid line), which shows a simple decrease after the specific frequency with the maximum electric field. The response without the layer is also plotted for the reference (0 km width).

The presence of the layer is found to have an effect to decrease the value of the electric field for any width, and as the layer becomes wider, we observe the weaker response. There is a characteristic frequency at which the maximum response is observed for all cases, and this

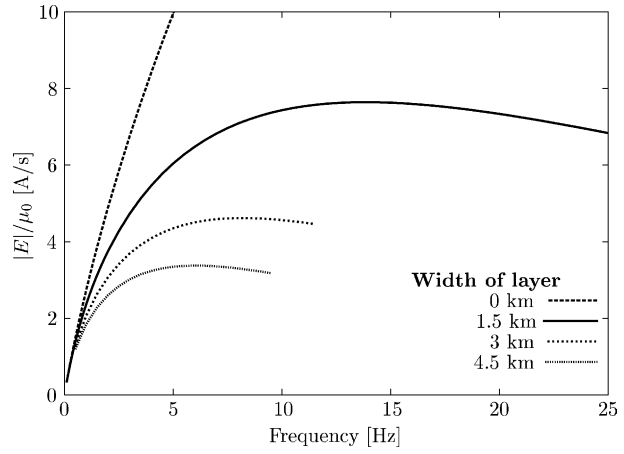

Fig. 3. Electric field at the ground surface and at the center of the layer for different layer thickness as a function of frequency. The source depth is 15 km.

frequency becomes lower as the layer is wider. We can conclude that there is an "optimal" frequency to measure the maximum ULF/ELF fields in the presence of the highly conductive layer if the source has a uniform frequency characteristic.

Fig. 4 shows the frequency characteristics of $|E|$ at some observation points for which the source is located outside the layer. For reference the $|E|$ for the inside source is also plotted. The width of the layer is 3 km, and the source is located at the depth of 15 km, but at $x = 4.5$ km, that is, the source is 3 km apart from the right boundary between the layer and the host medium. The other parameters used for this calculation are same as above.

It is observed that the responses in the side of the source with respect to the layer (the line indicated as 9 and 20 km), exhibit a simple increase and do not have the maximum frequency in this range, but if the observation point is within the layer or in the opposite side the curve has the maximum value, then decreases simply. This is the same tendency as the ones in Fig. 3. Even though the propagation path does not go across the layer, the response is influenced and is weaker than the case without the layer (see Fig. 3).

3.3. Influence of a highly conductive layer on spatial field distribution

The spatial profile of the electric field at the ground surface is shown in Fig. 5 as the ratio to one of the semi-space model. The calculation is performed for the case where the source is located inside and outside the layer. The necessary parameter for computation is the same as ones in the previous section, and the frequency is 7 Hz. The outside source position is apart from 70 km in $+x$-direction from the right boundary. The horizontal axis indicates the distance from the source, which means that for the case of the outside source, the layer ranges from -4.5 to -1.5 km, and for the inside source it ranges from -1.5 to 1.5 km.

For both cases the ratio is less than unity all over the shown range, and this tendency is held for all calculated frequency range (~20 Hz). Thus, the presence of a layer decreases the electric field for both the configurations. The ratio $|E|/|E_{\text{semi}}|$ is found to decrease with the decrease in frequency.

If the source is located outside the layer, then the electric field is stronger, in particular, on the side where the source is placed, and the larger response is observed even on another side. We can conclude that it is difficult to detect the ULF/ELF signals generated by the source inside the highly conductive layer.

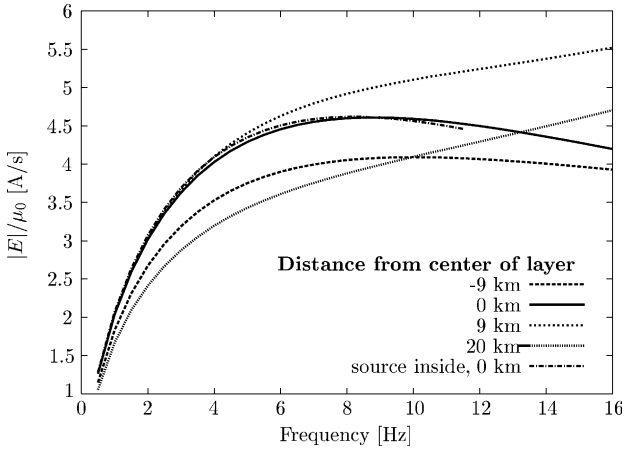

Fig. 4. Frequency characteristics of the electric field at the ground surface. The source is located at $x = 4.5$ and 15 km depth, and the thickness of the layer is 3 km.

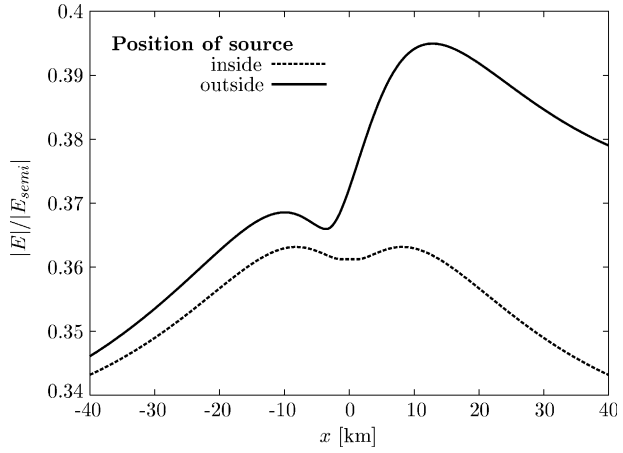

Fig. 5. Spatial distribution of electric field $|E|$ relative to the ones of the semi-space model, E_{semi} for the inside and outside source. The source position is $x = 0$.

3.4. Influence of subduction and sea water

We analyze the influence of subduction and sea water on the ULF/ELF electric field in this section. Fig. 6 illustrates the configuration for our analysis (Scholz, 1990). Sea water is simulated by a horizontal, thin, highly conductive layer and the top of the layer is located at the ground surface. Here the conductivity of sea water is set as 1 S/m, and the depth of sea is 1 km. The boundary between two geological plates is simulated by a conductive layer which exists obliquely. The top of the boundary is expressed by the equation:

$$y = \frac{2}{3}x - 10,$$

where both units of x and y are km, and the width and conductivity of the boundary are 5 km and 10^{-3} S/m, respectively.

Fig. 7 shows the spatial distribution of the electric field $|E|$ of the subduction area. We also plot the response without the oblique layer.

It is seen from the figure that the presence of the oblique layer decreases the intensity of the electric field as well as the one of the sea. We can also find that the maximum position of the electric field does not coincide with the source position, and it shifts from the source position by about 10 km.

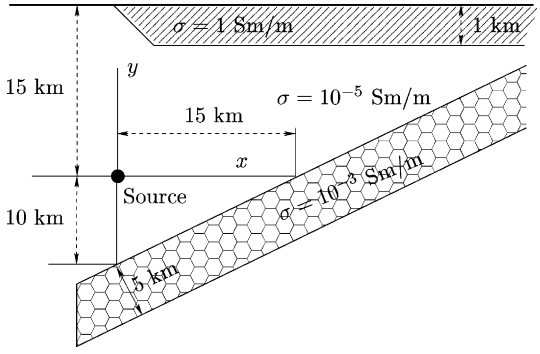

Fig. 6. Configuration for analysis in the subduction area.

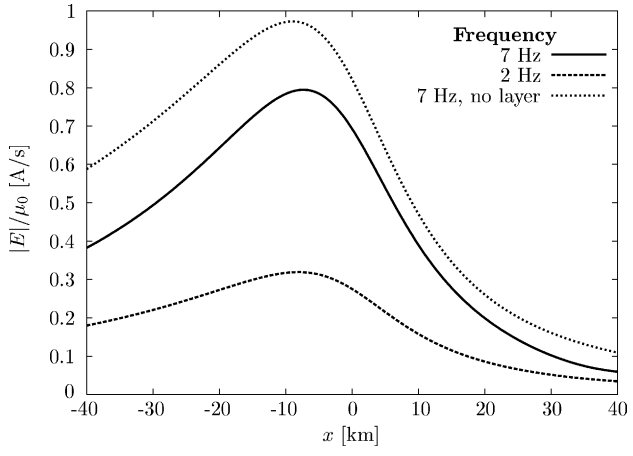

Fig. 7. Spatial distribution of electric field at the ground surface in the subduction area. The responses at two frequencies, 7 and 2 Hz, are plotted.

4. Conclusions

We have outlined the influence of highly conductive layers in the ground on the ULF/ELF electric fields generated by the line current source. It was shown that it is necessary to consider the semi-space model instead of the full-space model. There is a characteristic frequency in ULF/ELF ranges where the maximum of the electric field is obtained. This frequency depends on the conductivity and the thickness of the layer and can decrease the electric field response observed on the ground surface. However, in the case where the source is located outside the layer, the electric field increases, especially on the side of the source in comparison with the source inside the layer. A typical subduction area was studied as another situation. It was found that there is a big influence of sea water on the electric field on the ground surface. In this case the maximum of the electric field is not observed at the point closest to the source. It shows there exists the more appropriate point of the electric field observation for seismogenic ULF/ELF fields.

References

Fraser-Smith, A.C., Bernardi, A., McGill, P.R., Ladd, M.E., Helliwell, R.A., Vollard Jr., O.G., 1990. Low-frequency magnetic field measurements near the epicenter of the Ms7.1 Loma Prieta earthquake. Geophys. Res. Lett. 17, 1465–1468.

Gotoh, K., Akinaga, Y., Hayakawa, M., Hattori, K., 2002. Principal component analysis of ULF geomagnetic data for Izu islands earthquakes in July 2000. J. Atmos. Elect. 22, 1–12.

Hayakawa, M. (Ed.), 1999. Atmospheric and Ionospheric Electromagnetic Phenomena Associated with Earthquakes. Terrapub, Tokyo, p. 996.

Hayakawa, M., Fujinawa, Y. (Eds.), 1994. Electromagnetic Phenomena Related to Earthquake Prediction. Terrapub, Tokyo, p. 477.

Hayakawa, M., Molchanov, O.A. (Eds.), 2002. Seismo-Electromagnetics: Lithosphere–Atmosphere–Ionosphere Coupling. Terrapub, Tokyo, p. 447.

Hayakawa, M., Kawate, R., Molchanov, O.A., Yumoto, K., 1996. Results of ultra-low-frequency, Geophys magnetic field measurements during the Guam earthquake of 8 August, 1993. Geophys. Res. Lett. 23, 241–244.

Hayakawa, M., Itoh, T., Hattori, K., Yumoto, K., 2000. ULF electromagnetic precursors for an earthquake at Biak, Indonesia on February 17, 1996. Geophys. Res. Lett. 27, 1531–1534.

Hermance, J.F., 1995. Electrical conductivity models of the crust and mantle. In: Ahrens, T.J. (Ed.), Global Earth Physics: A Handbook of Physical Constants. American Geophysical Union, Washington DC, pp. 190–205.

Jin, J., 1993. The Finite Element Method in Electromagnetics. John Willey and Sons, New York. Appendix C, pp. 423–435.

Kopytenko, Y., Matiashvili, T.G., Voronov, Kopytenko, E.A., Molchanov, O.A., 1990. Ultra low frequency emission associated with

Spitak earthquake and following after shock activity using geomagnetic data at observatories Dusheti and Vardziya. Reprint of IZMIRAN, N3(888).

Molchanov, O.A., Hayakawa, M., 1995. Generation of ULF electromagnetic emissions by microfracturing. Geophys. Res. Lett. 22, 3091–3094.

Molchanov, O.A., Kopytenko, Y.A., Voronov, P.M., Kopytenko, E.A., Matiashvili, T.G., Fraser-Smith, A.C., Bernardi, A., 1992. Results of ULF magnetic field measurements near the epicenters of the Spitak ($M_s = 6.9$) and Loma Prieta ($M_s = 7.1$) earthquakes: comparative analysis. Geophys. Res. Lett. 19, 1495–1498.

Molchanov, O.A., Hayakawa, M., Rafalsky, V.A., 1995. Penetration characteristics of electromagnetic emission from an underground source into the atmosphere, ionosphere and magnetosphere. J. Geophys. Res. 100, 1691–1712.

Press, W.H., Teukolsky, S.A., Vetterling, W.T., Flannery, B.P., 2002. Numerical recipes in C++, 2nd ed. Cambridge University Press, Cambridge.

Sarlis, N., Lazaridou, M., Kapiris, P., Varotsos, P., 1999. Numerical model of the selectivity effect and the $\Delta V/L$ criterion. Geophys. Res. Lett. 26 (21), 3245–3248.

Scholz, C.H., 1990. The Mechanics of Earthquakes and Faulting. Cambridge University Press, Cambridge.

Tian, X., Hata, M., 1996. Analysis of seismogenic radiation and transmission mechanisms. J. Atmos. Elect. 16 (3), 227–235.

Uyeda, S., Hayakawa, M., Nagao, T., Molchanov, O.A., Hattori, K., Orihara, Y., Gotoh, K., Akinaga, Y., Tanaka, H., 2002. Electric and magntic phenomena observed before the volcano-seismo activity in 2000 in the Izu Island Region, Japan. Proc. US Natl. Acad. Sci.(PNAS) 99, 7352–7355.

Varotsos, P.N., Lazaridou, M., Kapiris, P., 1998. Transmission of stress induced electric signals in dielectric media. J. Appl. Phys. 83, 60–70.

Varotsos, P., Sardis, N., Skordas, E., 2000. Transmission of stress induced electric signals in dielectric media. Part 3. Acta Geophys. Polon. 48 (3), 263–297.